AN EVALUATION OF A BAKE-OUT OF THE ACIS INSTRUMENT ON THE CHANDRA X-RAY OBSERVATORY

Paul P. Plucinsky[a], Stephen L. O'Dell[b], Neil W. Tice[c], Douglas A. Swartz[d], Marshall W. Bautz[e], Joseph M. DePasquale[a], Richard J. Edgar[a], Gordon Garmire[f], Rino Giordano[g], Catherine E. Grant[e], Perry Knollenberg[g], Steve Kissel[e], Beverly LaMarr[e], Richard Logan[g], Martin Mach[g], Herman L. Marshall[e], Leon McKendrick[g], Gregory Prigozhin[e], Dan Schwartz[a], Norbert S. Schulz[e], Dan Shropshire[g], Tan Trinh[g], Alexey A. Vikhlinin[a], Shanil N. Virani[a]

[a]Harvard-Smithsonian Center for Astrophysics, 60 Garden St., Cambridge, MA 02138
[b]NASA Marshall Space Flight Center, Huntsville, AL 38512
[c] Lockheed Martin Space Systems, Denver, CO 80201
[d]Universities Space Research Association, MSFC, Huntsville, AL 35812
[e]Center for Space Research, Massachusetts Institute of Technology, Cambridge, MA 02139
[f]Department of Astronomy & Astrophysics, Pennsylvania State University, University Park, PA 16802
[g]Northrop Grumman Space Technologies, Redondo Beach, CA 90278

ABSTRACT

The sensitivity of the *Advanced CCD Imaging Spectrometer* (ACIS) instrument on the *Chandra X-ray Observatory* (CXO) to low-energy X-rays (0.3 - 2.0 keV) has been declining throughout the mission. The most likely cause of this degradation is the growth of a contamination layer on the cold (-60 C) filter which attenuates visible and near-visible light incident on the CCDs. The contamination layer is still increasing 4 years after launch, but at a significantly lower rate than initially. We have determined that the contaminant is composed mostly of C with small amounts of O and F. We have conducted ground experiments to determine the thermal desorption properties of candidate materials for the contaminant. We have conducted experiments to determine the robustness of the thin filter to the thermal cycling necessary to remove the contaminant. We have modeled the migration of the contaminant during this bake-out process to ensure that the end result will be a reduction in the thickness of the contamination layer. We have considered various profiles for the bake-out consisting of different temperatures for the ACIS focal plane and detector housing and different dwell times at these temperatures. The largest uncertainty which affects our conclusions is the volatility of the unknown contaminants. We conclude that bakeout scenarios in which the focal plane temperature and the detector housing temperature are raised to +20 C are the most likely to produce a positive outcome.

Keywords: CXO, Chandra, ACIS, Charge-Coupled Devices, CCDs, X-ray detectors, X-ray spectroscopy, molecular contamination, optical filters

1. INTRODUCTION

The *Chandra X-ray Observatory* (CXO) is the third of NASA's great observatories in space.[1,2] The CXO was launched on July 23, 1999 aboard the space shuttle *Columbia* on the STS-93 mission. The CXO was placed into a higher orbit by an Inertial Upper Stage (IUS) booster and then used its own propulsion system to achieve an

Further author information: (Send correspondence to P.P.P.)
P.P.P.: E-mail: plucinsky@cfa.harvard.edu, Telephone: 1 617 496 7726

UV and Gamma-Ray Space Telescope Systems, edited by Günther Hasinger, Martin J. L. Turner, Proceedings of SPIE Vol. 5488 (SPIE, Bellingham, WA, 2004) · 0277-786X/04/$15 · doi: 10.1117/12.552029

initial operating orbit with a perigee altitude of 10,000 km, an apogee altitude of 140,000 km, an inclination of 28.5° and a period of $\sim$ 64 hr. The CXO is controlled and operated by the Smithsonian Astrophysical Observatory (SAO) from Cambridge, Massachusetts. The *Chandra X-ray Center* (CXC), also run by the Smithsonian Astrophysical Observatory, processes and distributes *Chandra* data and provides analysis software and calibration products to the astronomical community.

The CXO carries two focal plane science instruments: the *Advanced CCD Imaging Spectrometer* (ACIS) and the *High Resolution Camera* (HRC). The Observatory also possesses two objective transmission gratings: the *Low Energy Transmission Grating* (LETG) that is primarily used with the HRC, and the *High-Energy Transmission Grating* (HETG) that is primarily used with the ACIS. ACIS was developed by a team from the Massachusetts Institute of Technology[3] and the Pennsylvania State University.[4,5] It contains two arrays of CCDs, one optimized for imaging and the other for spectroscopy as the readout detector for the HETG. The ACIS imaging array contains 4 Front-Illuminated (FI) CCDs configured in a 2×2 array and the spectroscopy array contains 2 Back-Illuminated (BI) CCDs and 4 FI CCDs configured in a 1×6 array. The focal point on the I array is on a FI CCD labeled "I3" and on the S array on a BI CCD labeled "S3".

2. DESCRIPTION OF THE ACIS HARDWARE

The ACIS instrument design is discussed in detail in several references.[4–6] The relevant pieces of the instrument for this paper are the focal plane (FP), the optical blocking filter (OBF), the detector housing (DH), and the collimator. A picture of the ACIS HW simulator is show in Figure 1. The arrangement of the CCDs in the focal plane is visible in this picture, the ACIS-I array CCDs are arranged in a 2×2 configuration and the ACIS-S array CCDs are arranged in a 1×6 configuration. The OBF is located $\sim$ 1.3 cm in front of the FP. The OBF consists of two distinct filters made of Al and polyimide (the OBF is not shown in Figure 1). The ACIS Imaging array OBF (OBF-I) is made of 1200 Å of Al, 2000 Å of polyimide, and 400 Å of Al, and the ACIS Spectroscopy array filter (OBF-S) is made of 1000 Å of Al, 2000 Å of polyimide, and 200 Å of Al. The top of the ACIS DH is visible in Figure 1 and is sometime referred to as the "snoot". The door (shown in the open position) provided a vacuum seal at the top of the DH prior to first light on 1999 August 12, and has subsequently remained open. The ACIS collimator is the structure surrounding the top of the DH and extends $\sim$ 30 cm from the top of the DH and $\sim$ 45 cm from the plane which contains the focal plane. The collimator is made of Ti and is coated with Au on the interior walls. The mounting feet for the collimator are visible in Figure 1 showing where the ACIS instrument is mounted onto the Science Instrument Module (SIM) in the CXO. Figure 2 (LEFT) shows the ACIS instrument mounted onto the SIM with the door closed. Figure 2 (RIGHT) shows the instrument with the door open. The OBFs are visible in this image.

The ACIS instrument has two heaters, one located on the FP and the other located on the side of the DH closest to the ACIS-S array. In normal operations, the FP temperature is maintained at -120 C and the DH temperature is maintained at -60 C. The top of the ACIS collimator is not regulated and its temperature is determined by the temperature at the location on the SIM. In flight, this temperature has averaged ~ -12 C. Therefore, there is a large gradient from the bottom of the collimator where the DH is located (-60 C) to the top of the collimator. In the first few months of the mission, the FP was held at higher temperatures (-100 C and -110 C), but the FP has been kept at -120 C since 29 January 2000 (except for a brief calibration period at -110 C in July 2000).

3. CHARACTERIZATION OF THE CONTAMINANT

The spectral response of the ACIS instrument has been evolving with time since the launch of CXO due to an increase in the charge-transfer inefficiency (CTI) of the CCDs and the development of a contamination layer on the filter. The effect of the CTI on the spectral response is discussed in numerous references elsewhere.[7–12] In this paper, we focus on the effect of the contamination layer.

The first evidence of the contamination layer was a higher-than-expected depth in the C-K edge (an absorption edge produced by the K shell in neutral C at $\sim$ 0.284 keV) in an 1999 gratings observation of the narrow-line Seyfert galaxy Ton S 180 (see Marshall *et al.* 2004[13]). At this point, there were no data on the time-dependence of this increased absorption and it was assumed that the effect was constant in time and was attributed to

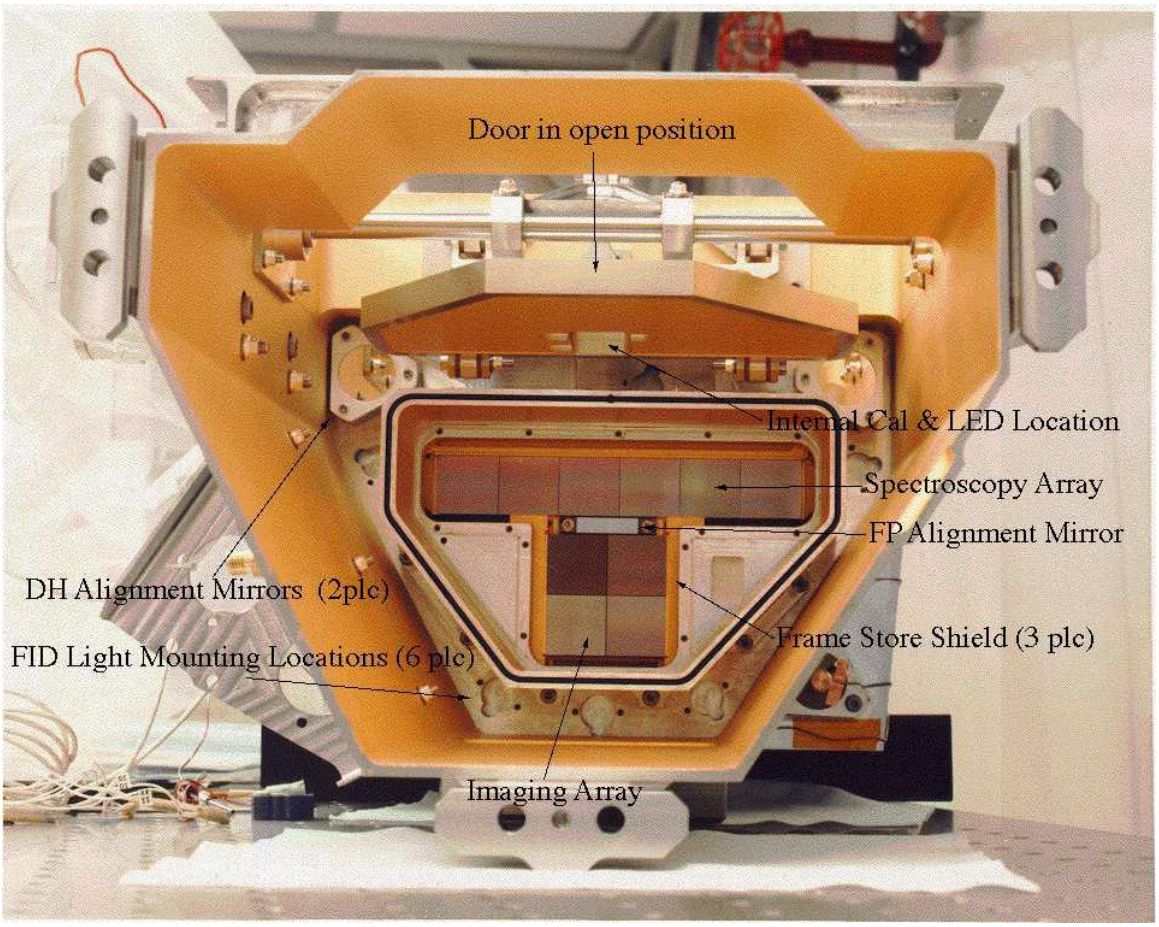

Figure 1. A picture of the ACIS HW simulator. The picture is taken looking down the ACIS collimator towards the ACIS detector housing and the focal plane. The ACIS door is shown in the open position. Ten CCDs are shown installed in the focal plane, but an OBF is not installed in this unit. A CCD is 2.5 cm on a side and the distance from the top of the collimator to the focal plane is ~ 45 cm. The major difference between the HW simulator and the flight unit is the cutout on the side of the collimator closest to the door mechanism which is closed off in the flight unit.

an incorrect calibration of the OBF-S transmission. Over the following years, it became clear that the count rates from non-variable sources with soft X-ray spectra were decreasing in time. In the subsequent analyses, it became clear that the depth of the C-K edge was increasing in time over the course of the mission. It was also discovered that additional absorption was present at the O-K and F-K edges.[13] Finally, it was demonstrated that both the ACIS-I and and ACIS-S arrays were suffering a similar decrease in sensitivity. Since the effect is increasing in time and there is no F in the ACIS OBF, the explanation could not be an error in the OBF transmission models. Given that the ACIS DH and FP are the coldest surfaces interior to the CXO spacecraft, the likely explanation was that a layer of contamination was accumulating on the OBF and/or the FP. This contamination layer introduces an additional absorption component which reduces the detection sensitivity of the ACIS instrument at energies less than 2 keV.

3.1. TIME DEPENDENCE OF THE ACCUMULATION OF THE CONTAMINANT

The ACIS instrument contains an external calibration source (ECS) which provides fluorescence X-rays at Al-K α (1.49 keV), Ti-K α (4.5 keV), and Mn-K α (5.9 keV). In addition to the relatively stronger K α lines, there are weaker lines from L shell emission from Mn and Fe. The ratio of the Mn-L & Fe-L complex and the Mn-K complex provides a useful diagnostic of the thickness of the contamination layer with time, since the

Figure 2. (LEFT) The ACIS instrument mounted onto the SIM looking down toward the FP. The ACIS door is closed. The darker structures above the collimator are the SIM aperture and part of the SIM focus structure. (RIGHT) The ACIS instrument with the door open. The OBFs are installed and visible in this picture. The wrinkles in the spectroscopy array OBF are typical and do not affect the performance of the filter.

Mn-L & Fe-L X-rays are attenuated much more severely than the Mn-K X-rays, which are mostly unaffected. The ratio of the Mn-L & Fe-L and Mn-K lines is independent of the radioactive decay of the Fe55 source itself. Figure 3 shows the value of this ratio for the first 1800 days of the CXO mission. The ratio has been declining throughout the mission but the rate of decline has been slowing, perhaps indicating that the accumulation rate of the contaminant is also slowing. We have fit these data with the function:

$$(\text{Mn L} + \text{Fe L})/\text{Mn K ratio} = \text{N}_\text{o} \times exp[-\tau_\infty \times (1 - exp(-t/t_o))] \quad (1)$$

where N_o is the value of the ratio at $t = 0$, t is the number of days since launch, τ_∞ is the optical depth at the effective energy of the Mn-L complex ($\sim$ 670 eV) at $t = \infty$, and t_o is a characteristic time constant. Since this function is an exponential of an exponential decay in time, we cannot interpret the value of t_o as the characteristic time constant of the overall decay. The solid line plotted in Figure 3 is this model with the following parameters, $\text{N}_\text{o} = 0.0072$, $t_\infty = 0.582$, and $t_o = 620$ d. The asymptotic value of this function is 0.00403. If this model can be legitimately extrapolated into the future, this implies that $\sim 95\%$ of the decrease in the ratio has already occurred.

3.2. ENERGY DEPENDENCE OF THE CONTAMINANT ABSORPTION

The chemical composition of the contaminant has been well-characterized by gratings observations of bright, continuum sources. Marshall *et al.* 2004[13] have determined that the contaminant is composed mostly of C with small amounts of O and F. The C:O ratio is 11.5:1 and the C:F ratio is 14:1. N is not detected in the contaminant, with an upper limit of 3% of the total contaminant. The contaminant most likely also includes hydrogen, since the contaminant is most likely a hydrocarbon. But the CXO bandpass is rather insensitive to absorption from H with a K edge at 0.13 keV.

The *Chandra X-ray Center* (CXC) has constructed a time-dependent model of the additional absorption produced by the contamination layer to be used in the analysis of CXO data. Figure 4 displays the effective area of the HRMA/ACIS-S3 configuration at launch and at May, 2004. The decrease in effective area at energies below 2 keV is apparent and is due entirely to the additional absorption caused by the contamination layer.

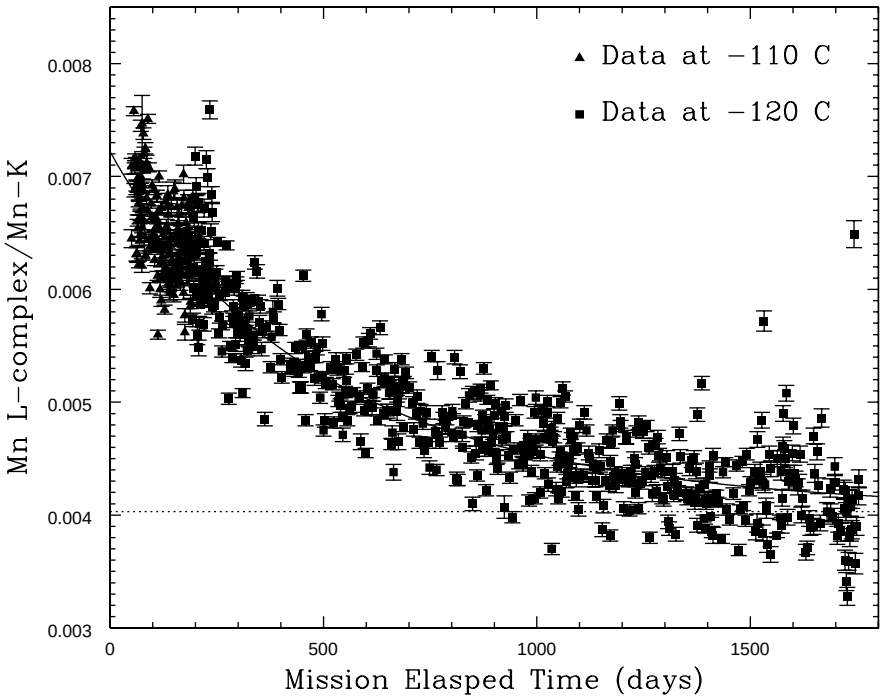

Figure 3. The ratio of the Mn L & Fe L complex/Mn K complex versus time from the S3(BI) CCD. The data collected with the focal plane at -110 C are indicated by the triangles and the data collected at -120 C are indicated by the squares. The solid line is a model of the time dependence in Eqn. 1 and the dashed line is the asymptotic value of 0.00403.

Notice that there is not a significant change to the effective area at energies above 2 keV. Figure 4 also displays the fractional difference in the launch effective area and the May, 2004 effective area. The effective area values are based on the model described above. The absorption edges produced by the C, O, and F, in the model of the contaminant are indicated in the figure.

3.3. SPATIAL DISTRIBUTION OF THE CONTAMINANT

The thickness of the contaminant is observed to vary with position. The contaminant is measured to be thicker at those locations on the CCD underneath the edges of the OBFs and the contaminant is measured to be thinner at those locations on the CCD underneath the centers of the OBFs. Thermal models of the OBFs indicate that there is a significant temperature gradient across the OBFs (see 4.2), with the centers warmer than the edges by $4.5-7.5°$. The obvious interpretation of the variation in the contaminant thickness is that the colder surfaces of the OBFs have accumulated more contaminant than the warmer surfaces. We have assumed that the majority of the contaminant is on the OBF and not on the CCDs. Figure 5 shows the measured optical depth at ~ 0.7 keV at the center and edge of the S3 CCD based on the analysis of the ECS data. The difference in the optical depth is about 0.27 in the middle of 2004. This difference is significant given the statistical uncertainties.

3.4. MATERIALS INVESTIGATION

Hydrocarbon contaminants are common in vacuum and spacecraft applications. The identification of a contaminant which was composed mostly of C was not useful in identifying candidate materials on the spacecraft. However, the number of materials on the CXO which contain F is reasonably small. Once the F had been detected in the ACIS contaminant, the CXO spacecraft contractor (*Northrup-Grumman Space Technologies*, formerly known as TRW) reviewed the list of candidate materials and selected several for additional testing. There are two fluorocarbon-based lubricants used on the CXO, Braycote in the SIM translation mechanism

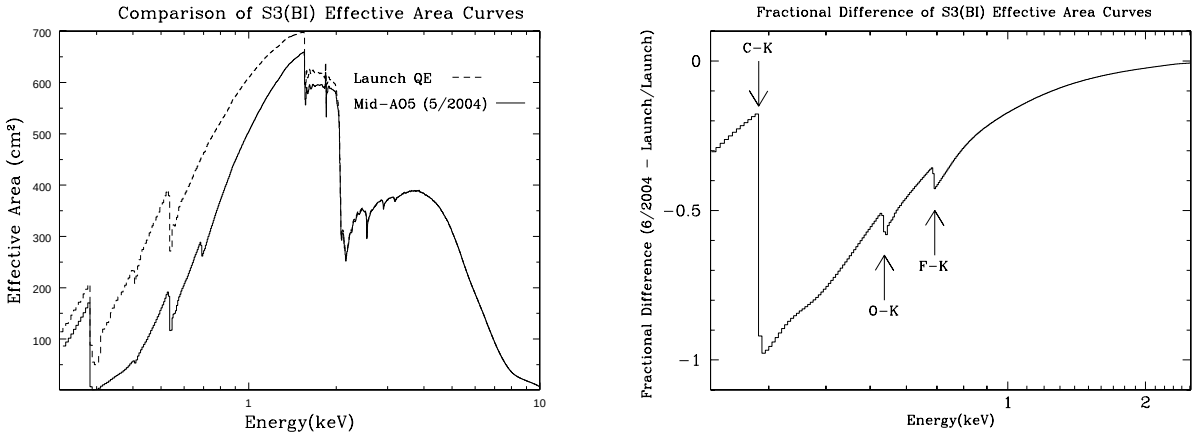

Figure 4. (LEFT) The effective area of the HRMA/ACIS-S3 configuration at launch and at May, 2004. (RIGHT) The fractional difference of the HRMA/ACIS-S3 effective area at launch and at May, 2004 as predicted by the CXC model. The absorption edges in the model due to C, O, and F are labeled in the figure.

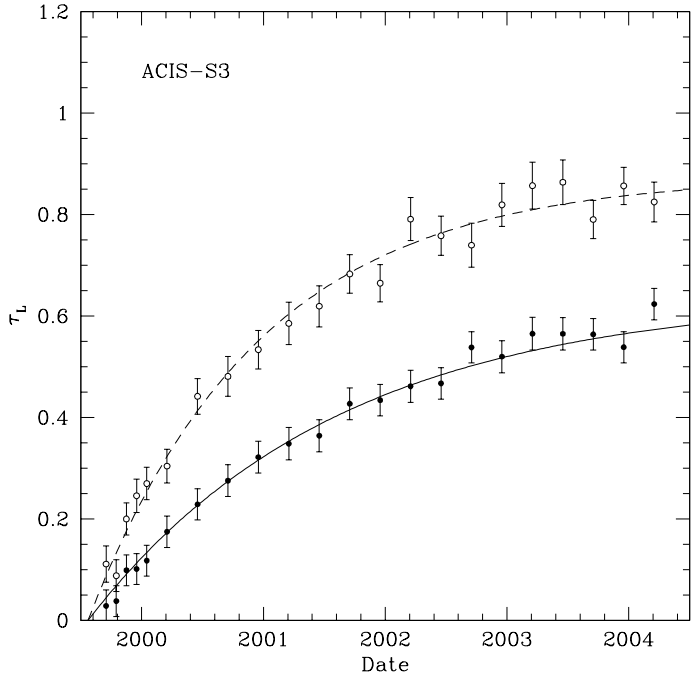

Figure 5. The optical depth of the contaminant as measured at ~ 0.67 keV using the ECS data for the center (open circles) and bottom (filled circles) of the S3 CCD.

and Krytox in the gratings insertion and retraction mechanisms. Samples of the candidate materials were subjected to a Gas-Chromatography/Mass-Spectroscopy (GC/MS) analysis and the relative concentrations of C, O, and F were measured. None of the candidate materials had the observed ratios of C, O, and F in the ACIS contaminant. Since some materials had lower ratios of C:F and there are many materials on the spacecraft which contain C but no F, it was concluded that the ACIS contaminant is most likely a mixture of two or more materials. From the measured C:F = 14, only a small fraction ($\sim 3\%$) of the contamination could be a pure fluorocarbon.

Samples of the Braycote lubricant were tested further to determine the thermal desorption properties of the material in a *Vacuum Outgassing/Deposition Kinetics Apparatus*. A sample of Braycote was heated to a relatively high temperature (typically +150 C), allowed to out-gas onto a cold (typically -60 C or -190 C) Quartz-Crystal Micro-balance (QCM), and then the QCM was heated to determine the rate at which the material desorbed. It was noticed that the Braycote sample outgassed very little at +150 C and it was difficult to collect a significant mass on the QCM. Braycote samples were then irradiated with 0.5-4.0 Mrad from a ^{60}Co source and heated to +150 C. It was noticed that the irradiated Braycote outgassed at a significantly higher rate, presumably because the radiation had converted some of the high molecular weight material to lower molecular weight material. The out-gassing products of the irradiated Braycote were then subjected to the same thermal desorption tests. It was found that about half of the material sublimated when the QCM was heated from -60 C to +20 C within 2 hr and the rest of the material sublimated very slowly. It took an additional $\sim$ 35 hr for the thickness of the material on the QCM to reduce by another factor of two. We conclude from this that the outgassing products of irradiated Braycote heated to +150 C contain a mixture of materials with a range of volatilities. Fortunately, there is no internal part of the CXO spacecraft which has reached temperatures of +150 C. The outgassing products probably contained high molecular weight materials which have not outgassed on the CXO spacecraft. Nevertheless, these tests were useful to bound the range of possible volatilities for irradiated Braycote.

The near-edge absorption structure of the contaminant can be used to constrain the molecular structure of the contaminant as reported previously.[13] The contaminant on the ACIS OBF is most consistent with an aliphatic hydrocarbon, containing only C-C single bonds. The absorption spectrum is inconsistent with an aromatic hydrocarbon, containing C=C double bonds.

4. SIMULATIONS OF THE BAKEOUT

In order to investigate migration of the molecular contamination during bakeout, we developed simulation software (to be described in detail elsewhere). The simulation software takes as input for each node geometric information (area and view factor — i.e., visibility of each node from any other node), temperature, initial column density of contaminant, and relevant properties of the contaminant. Because we have not been able to identify uniquely the contaminant(s), we necessarily consider a range of temperature-dependent volatilities.

4.1. PHYSICAL MODELS OF ACIS AND THE SIM

Geometric models of the ACIS instrument were developed at Lockheed-Martin (formerly Martin-Marietta) during the instrument development using the Thermal Radiation Analysis System (TRASYS) software. Physical models of the SIM and spacecraft were developed at Ball Aerospace and Northrup-Grumman during the SIM and spacecraft development. These models were resurrected and modified to give higher resolution for this effort to provide an accurate description of the relevant physical surfaces.

4.2. THERMAL MODELS OF ACIS AND THE SIM

The TRASYS output also gives radiation conductor coefficients, which the thermal-network analyzer (SINDA) solves to determine the temperature of each node. The temperatures had already been modeled for the nominal operations case in which the ACIS FP is at -120 C and the DH is at -60 C. For the modeling of the bakeout, we desired the capability to examine FP temperatures between -120 C and +20 C and DH temperatures between -60 C and +20 C and to determine the resulting temperatures of the OBFs. For this purpose, the model needed to be updated to include more nodes on the OBFs. In normal operations, there is a gradient from -60 C at the bottom of the ACIS collimator (where the DH and FP are located) to -12 C at the top of the collimator where the instrument attaches to the SIM. When the DH bakeout heater is used, the DH rises to a temperature range of +17.5 to +22.5 C (there is a gradient from one side of the DH to the other given that the heater is on one side). This reverses the gradient along the collimator such that the bottom is at $\sim$ +20 C and the top remains at -8 C. Figure 6 shows a map of the temperature distribution across the ACIS collimator.

During initial simulations of the bakeout, it was discovered that a large fraction of the contaminant migrated to the top of the ACIS collimator and the nearby SIM aperture, and remained there for long timescales. The

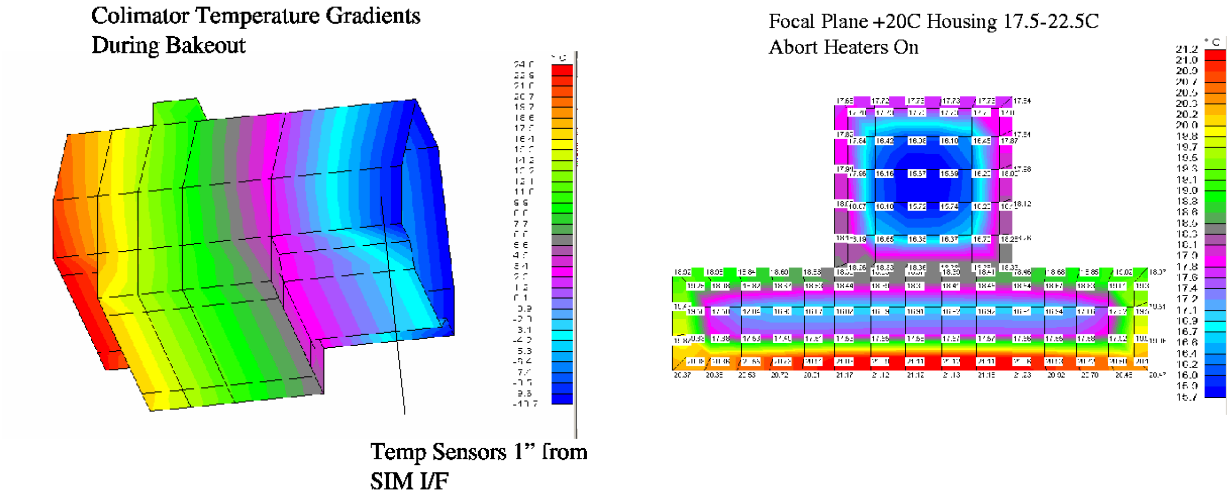

Figure 6. (LEFT) ACIS collimator temperatures during bakeout with the SIM abort heaters off. Note the bottom of the collimator is towards the left and the top of the collimator is towards the right. (RIGHT) The temperature distribution across the ACIS OBFs during bakeout with the FP=+20 C, the DH=+20 C and the SIM aperture at +10 C.

unfortunate consequence of this was that the contaminant would return to the OBF once the FP and DH had returned to their normal operating temperatures. We examined the impact of turning on additional heaters on the SIM to warm the SIM aperture and top of the ACIS collimator. The thermal models indicate that these surfaces would reach a temperature of $\sim$ +10 C. In this case, the gradient across the collimator would be significantly smaller, from +20 C at the bottom to +10 C at the top.

We also modeled in detail the temperature gradient across the OBFs. In normal operation, the edges of the filters are at -60 C and the center of the OBF-I is -52.7 C and the center of the OBF-S is -55.4 C. If the FP is heated to +20 C, the DH to +20 C, and the SIM aperture to +10 C, the center of the OBF-I filter rises to +15.7 C and the center of the OBF-S filter rises to +17.0 C. As will become apparent in the next section, it is crucial to get the OBFs as warm as possible and as close to the temperature of the DH as possible. Figure 6 shows a map of the temperature distribution across the OBFs for these bakeout conditions.

4.3. SIMULATIONS OF THE BAKEOUT

The *Chandra* project developed two sets of simulation software to model the effectiveness of a bakeout of the ACIS instrument. The first set was developed by NGST based on the physical and thermal models from TRASYS and contaminant migration using the CONFLUX/MOLFLUX software (CONFLUX is proprietary NGST SW), which uses a sticking-factor simulation of the contamination migration. The NGST model adopted the thermal desorption profile of the Braycote samples as a model for the contaminant properties. NASA MSFC developed a second set of software to study the contamination migration. This simulation software solves the time-dependent evolution of the contaminant's mass column for each node based upon its temperature-dependent vaporization rate and deposition from other nodes. The Clausius-Clapeyron equation was used to relate the vapor pressure at -60 C to the vapor pressure at +20 C, and temperatures in between. The MSFC model contained more nodes in the ACIS instrument and on the OBFs and was more flexible at tracking the mass on each surface as a function of time during the bakeout.

Both sets of simulation SW gave qualitatively similar results. Both indicated that a bakeout with the FP temperature significantly below room temperature was unlikely to provide a satisfactory result, since the centers of the OBFs would be significantly colder than the surrounding surfaces of the DH. It was assumed that the contamination layer is present on all surfaces close to -60 C, including the interior walls of the DH which have a large view-factor of the filter. As the contaminant vaporizes from the interior walls of the DH, a large fraction

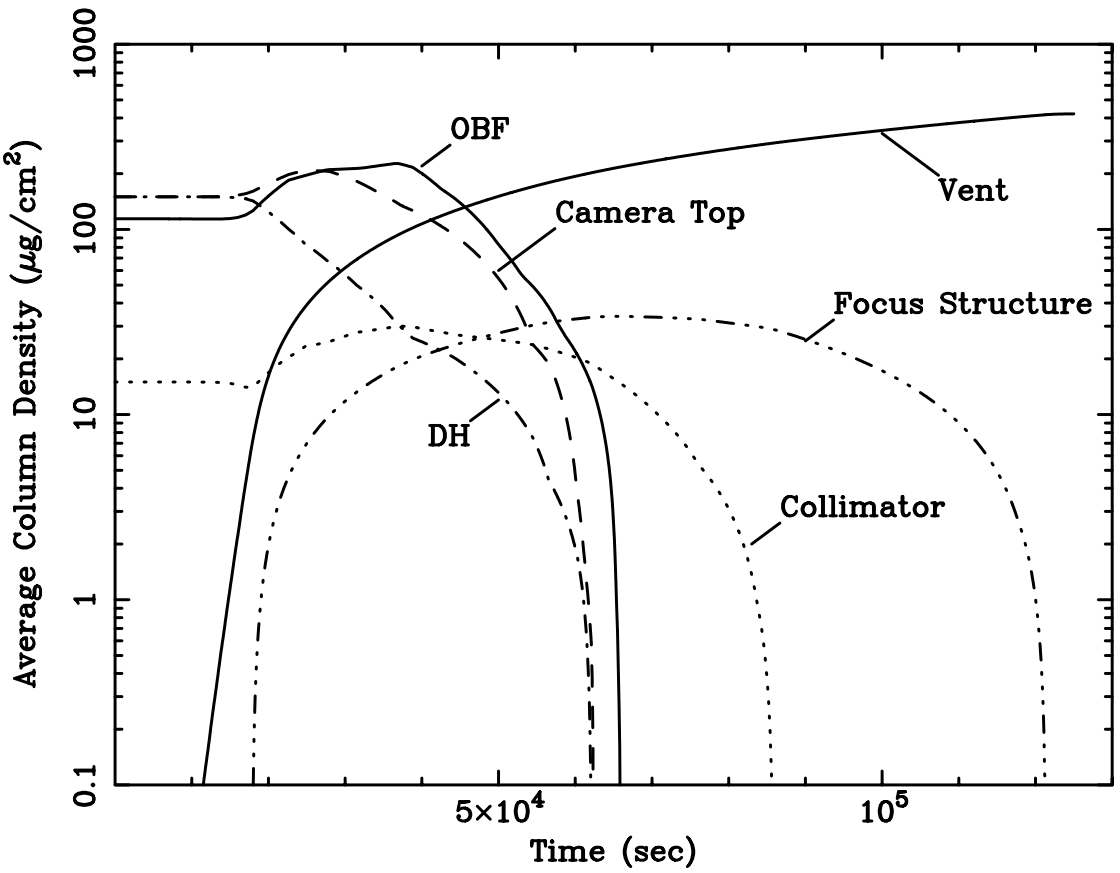

Figure 7. The average column density on the selected surfaces during the nominal, FP=+20 C, DH=+20 C bakeout as a function of time. The line labeled "vent" indicates material which has vented out the spacecraft.

of that material deposits on the centers of the OBFs. If the centers of the OBFs are much colder than the DH walls, the material will remain on the OBFs for a long time before vaporizing.

The MSFC bakeout model allows us to track the mass on any surface as a function of time during the bakeout. Figure 7 shows the time history of the column density of the contaminant on 9 reference surfaces in the model for a DH=+20 C and FP=+20 C bakeout. For simulation of this "nominal" case, we assume a contaminant of intermediate volatility, which would already show signs of vaporizing at -50 C, and extrapolate the mass vaporization to other temperatures using a vaporization enthalpy of 90 kJ/mole. In the beginning of the bakeout, all of the material is on the ACIS DH and OBF. As the surfaces are heated, the contaminant vaporizes from the DH and OBF and migrates to the top of the collimator and the SIM focus structure. The contaminant continues migrating to the Optical Bench Assembly (OBA) and eventually out the satellite. The SIM focus structure is the last surface to clean up since it is the coldest surface in the system. For this model run, all of the contaminant is removed from the OBF and vents overboard in 1.3×10^5 s. A bakeout of this duration could be easily accommodated within the 1.7×10^5 s viewing time available during a single *Chandra* orbit.

In order to assess the robustness of this model prediction, we have executed another model run in which the temperatures of all surfaces were reduced by 2.5° and the mass vaporization rate was reduced by half. This "off-nominal" run indicated that a complete removal of the contaminant would take three times longer ($\sim 4.0 \times 10^5$ s). While this indicates the sensitivity of the bakeout time to temperatures and vaporization rates, ultimately incomplete characterization of the contaminant(s) limits the accuracy of the simulation. The simulation software is an effective tool for evaluating the relative efficacy of bakeout scenarios; however, without

knowledge of the contaminant's vaporization rate, absolute time scales remain uncertain.

We also investigated the effect of keeping the FP colder than +20 C. In these runs, the centers of the OBFs are colder and accumulate material during the bakeout. Only after all of the material has been removed from the walls of the DH does the column density on the OBFs begin to drop. Figure 8 shows the average column density on the OBFs as a function of time for FP temperatures of -60 C, -20 C, 0 C, and +20 C. One interesting result of these model runs is the large increase in the OBF column density in the early stages of the bakeout. Once the deposition of material onto the OBF has ceased, it then takes a characteristic time for that material to vaporize based on the temperature of that surface. This figure indicates that a bakeout with the FP at -60 C is simply not feasible. A bakeout with the FP at -20 C would require over 100 hours for a complete removal of the contaminant from the OBF (with additional time for the contaminant to vent out of the spacecraft), while a bakeout with the FP at +20 C would require about 20 hr for a complete removal from the OBF. Based on these simulation results, we conclude that the FP must be warmer than +10 C and hence the centers of the OBFs within 10° of the DH temperature for the bakeout to be successful within one orbit of the CXO.

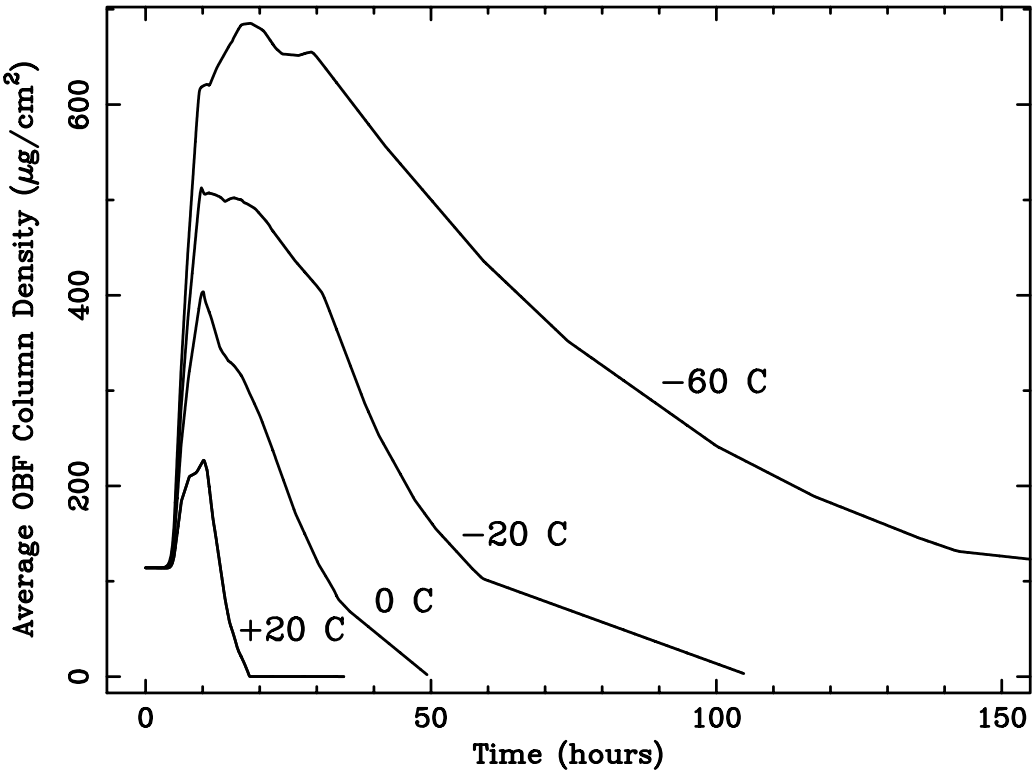

Figure 8. The average column density versus time on the OBFs for bakeouts with FP temperatures of -60 C, -20 C, 0 C, and +20 C.

These results emphasize the three main concepts for a successful bakeout. First, the surface to be cleaned needs to be heated to as warm a temperature as is possible and/or desirable. Second, the surface to be cleaned should be warmer than any other surface in the system to ensure that the surface of interest is not cross-contaminated during the bakeout. Third, the bakeout needs to be of sufficient duration to allow adequate time for the contaminant(s) to vaporize from the all surfaces, migrating through the Observatory and venting completely.

5. RISK ASSESSMENT

As with any contingency action on any spacecraft, a bakeout of the ACIS instrument contains some element of risk. We have analyzed the five risk items below.

5.1. THERMAL CYCLING DAMAGES THE ACIS HARDWARE

The ACIS instrument was designed to be thermally cycled. The instrument was thermally cycled from a cold FP temperature to +30 C over 40 times on the ground in pre-launch testing. The instrument has been thermally cycled to a FP temperature of +30 C and DH temperature of +20 C twice on orbit. There appears to be minimal risk to the instrument from the proposed bakeout thermal cycles.

5.2. DAMAGE TO THE OBF

The ACIS OBFs were thermally cycled many times on the ground and twice in orbit. The concern arises that a thick layer of contaminant on the OBF would change the mechanical properties such that the OBF would be more susceptible to damage from the thermal cycles. To address this concern, flight spare OBFs (one OBF-I and one OBF-S) were tested at NGST. The tests consisted of depositing a thick layer of contaminant on the OBFs and then thermally cycling the OBFs 40 times. CALWAX 170 was selected as a surrogate for the flight contaminant since it would desorb slowly at +25 C but sufficiently fast at +50 C to allow cleanup of the OBFs. Two tests were conducted to simulate a FP=+20 C bakeout and a FP=-60 C bakeout. A vacuum chamber was modified at NGST to simulate the relevant surfaces in the ACIS instrument to produce the desired temperature gradients across the OBFs. In the FP=+20 C bakeout tests, a layer of $118\mu g/cm^2$ was deposited on the OBFs and then the OBFs were cycled from -60 C to +25 C 40 times. The OBFs were then heated to +50 C to remove the contaminants and cycled an additional 5 times to ensure that the OBFs could survive thermal cycling once the contaminant has been removed. In the FP=-60 C bakeout, a layer of $180\mu g/cm^2$ was deposited on the OBFs and then the OBFs were cycled from -60 C to +25 C 40 times. The OBFs were then heated to +60 C to remove the contaminants and cycled five more times. At the conclusion of these tests there was no visible damage to the OBFs. We conclude from these tests that thermally cycling the OBFs with a thick layer of contaminant poses little risk.

5.3. LARGER THAN EXPECTED INCREASE IN CTI

The second FP=+30 C bakeout of the ACIS instrument in September 1999 resulted in a $\sim 30\%$ increase in the CTI of the FI CCDs. A possible mechanism for the bakeout-induced CTI increase is discussed in Kono *et al.*.[14] It appears likely that another bakeout with the FP close to room temperature will increase the CTI of the FI CCDs. The effectiveness of the bakeout must be evaluated against the possible CTI increase of the FI CCDs. An increase of 30% would be undesirable but would not seriously impact the capabilities of the CXO. CTI increases much larger than 30% would begin to impact the 15 year lifetime goal of the CXO. An extreme CTI increase of 300% would result in half the charge from an X-ray charge packet being lost after 1024 transfers from the top of the CCD. Such an increase would result in the FI CCDs not being useful for imaging near the top of the CCDs. We believe that CTI increases of a factor of two or more are extremely unlikely based on ground testing of irradiated CCDs and theoretical arguments. However, CTI increases up to 30% are certainly plausible. Figure 9 shows the full-width at half-maximum (FWHM) of the I3 CCD from February 2000 and May 2004 with a CTI-correction algorithm applied. The performance without the CTI correction is also shown for reference. We have estimated the impact 15% and 25% CTI increases would have on spectral resolution. Such increases in the CTI would result in a $10-18\%$ increase in the FWHM at the top of the FI CCDs and $3-5\%$ at the top of the S3 CCD. Such increases are clearly tolerable and would not gravely impact the science mission of the CXO.

5.4. UNDESIRABLE CHANGE IN THE CONTAMINATION LAYER

It is possible that a bakeout will result in a thicker layer of the contaminant on the OBF. The most effective means to prevent this from occurring is to keep the OBFs warmer than the surrounding surfaces. However, given the trade between bakeout effectiveness and the CTI increase, a bakeout with the FP=+20 C offers the best compromise between the two objectives. It is also possible that the contaminant might migrate to a cold surface and then redeposit quickly once the FP is cooled back down. The likelihood of such an outcome is minimized by warming all the surfaces within ACIS and the SIM aperture to close to +20 C so that the contaminant vents quickly to the OBA. Finally, the contaminant might migrate to another spacecraft system and cause problems for that system. This appears unlikely since all the spacecraft systems have been exposed to the contaminant

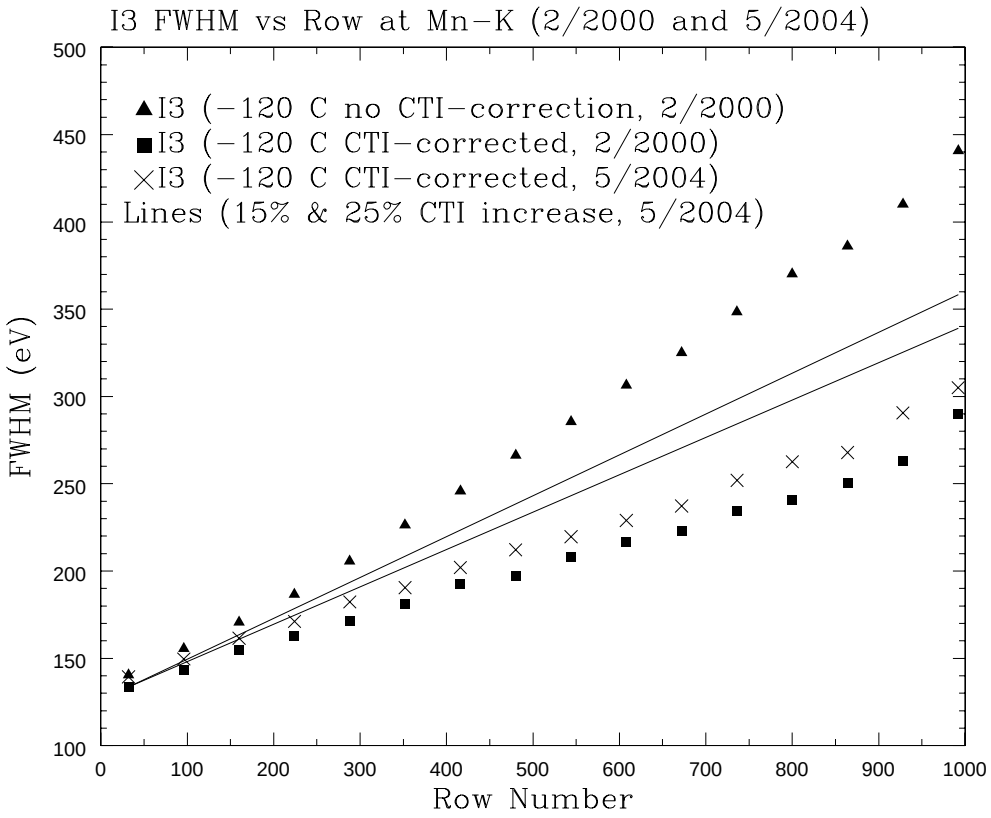

Figure 9. The FWHM of the ACIS I3 detector versus row number with and without a CTI correction for Mn Kα X-rays (5.9 kev) at February 2000 and May 2004. The solid lines are the predicted increase in FWHM for CTI increases of 15% and 25%.

for the last 5 years and they have not experienced any ill effects, presumably because the surfaces in those systems are too warm for the contaminant to accumulate.

5.5. THERMAL CYCLING DAMAGES ANOTHER SPACECRAFT SUBSYSTEM

The CXO Flight Operations Team (FOT) has evaluated the risk of increasing the temperature of the SIM aperture. The proposed temperature increase is below the ground testing limits and far below the design limits of the SIM. The additional SIM heaters which are proposed to be used have not been exercised since launch. The CXO FOT is evaluating the risks associated with using these heaters at this time.

6. CONCLUSIONS

We have determined that a bakeout of the ACIS instrument with the FP=+20 C and the DH=+20 C for 1.5×10^5 s is likely, but not guaranteed, to significantly reduce the contamination layer on the OBF. This result is based on two independent modeling efforts with different assumptions. The largest uncertainty in this analysis is the volatility of the contaminant(s). The contamination is most likely a mixture of materials, each with its own desorption properties. The success of the bakeout will depend on these properties. The most significant risk of the bakeout is a possible increase in the CTI of the FI CCDs with a subsequent decrease in the spectral resolution. The benefit of a possible bakeout must be weighed against this risk. The *Chandra* project is considering this tradeoff at the present time.

ACKNOWLEDGMENTS

This work was supported by NASA contract NAS8-39703.
We thank Harvey Tananbaum, Martin Weisskopf, Adam Hitchcock, Robert Goeke, William Mayer, Edward Boughan, Peter Ford, Leisa Townsley, George Chartas, Kelly Henderson, Kenny Chen, John Lamb, Lorraine Ryan, Fred Cottrell, Andy Tao, Lee Harper, Dan McGregor, Allyn Tennant, Ronald Elsner, and Hien Tranh. We thank all of our colleagues on the CXO project who have contributed directly or indirectly to this work.

REFERENCES

1. M. C. Weisskopf, H. D. Tananbaum, L. P. Van Speybroeck, and S. L. O'Dell, "Chandra x-ray observatory (cxo): overview," in *X-Ray Optics, Instruments, and Missions III*, J. E. Truemper and B. Aschenbach, eds., *Proc. SPIE* **4012**, p. 2, 2000.
2. M. C. Weisskopf, B. Brinkman, C. Canizares, G. Garmire, S. Murray, and L. P. Van Speybroeck, "An overview of the performance and scientific results from the chandra x-ray observatory," *Publications of the Astronomical Society of the Pacific* **114**, p. 1, jan 2002.
3. M. Bautz, M. Pivovaroff, F. Baganoff, T. Isobe, S. Jones, S. Kissel, B. Lamarr, H. Manning, G. Prigozhin, G. Ricker, J. Nousek, C. Grant, K. Nishikida, F. Scholze, R. Thornagel, and G. Ulm, "X-ray ccd calibration for the axaf ccd imaging spectrometer," in *X-Ray Optics, Instruments, and Missions*, R. B. Hoover and A. B. W. II, eds., *Proc. SPIE* **3444**, p. 210, 1998.
4. G. P. Garmire, M. W. Bautz, P. G. Ford, J. A. Nousek, and G. R. Ricker, "Advanced CCD imaging spectrometer (ACIS) instrument on the Chandra X-ray Observatory," in *X-Ray and Gamma-Ray Telescopes and Instruments for Astronomy*, J. Truemper and H. Tananbaum, eds., *Proc. SPIE* **4851**, pp. 28–44, Mar. 2003.
5. G. Garmire, G. Ricker, M. Bautz, B. Burke, D. Burrows, S. Collins, J. Doty, K. Gendreau, D. Lumb, and J. Nousek, "The axaf ccd imaging spectrometer," in *American Institute of Aeronautics and Astronautics Conference*, p. 8, 1992.
6. E. A. Boughan, J. P. Doty, R. F. Foster, D. A. Gong, G. G. andGordon, and N. Tice, "ACIS focal plane instrument for the AXAF-I spacecraft," in *AIAA, Space Programs and Technologies Conference*, 1994.
7. G. Prigozhin, S. Kissel, M. Bautz, C. Grant, B. LaMarr, R. Foster, G. Ricker, and G. Garmire, "Radiation damage in the chandra x-ray ccds," in *X-Ray Optics, Instruments, and Missions*, J. E. Truemper and B. Aschenbach, eds., *Proc. SPIE* **4012**, p. 720, 2000.
8. G. Prigozhin, S. Kissel, M. Bautz, C. Grant, B. LaMarr, R. Foster, and G. Ricker, "Characterization of the radiation damage in the chandra x-ray ccds," in *X-Ray Optics, Instruments, and Missions*, K. A. Flanagan and O. H. Siegmund, eds., *Proc. SPIE* **4140**, p. 123, 2000.
9. L. K. Townsley, P. S. Broos, G. P. Garmire, and J. A. Nousek, "Mitigating charge transfer inefficiency in the chandra x-ray observatory advanced ccd imaging spectrometer," *Astrophysical Journal* **534**, pp. L139–LL142, 2000.
10. L. K. Townsley, P. S. Broos, J. A. Nousek, and G. P. Garmire, "Modeling charge transfer inefficiency in the chandra advanced ccd imaging spectrometer," *Nuclear Instruments and Methods* **486**, p. 751, 2002.
11. L. K. Townsley, P. S. Broos, G. Chartas, E. Moskalenko, J. A. Nousek, and G. G. Pavlov, "Simulating ccds for the chandra advanced ccd imaging spectrometer," *Nuclear Instruments and Methods* **486**, p. 716, 2002.
12. P. P. Plucinsky, N. S. Schulz, H. L. Marshall, C. E. Grant, G. Chartas, D. Sanwal, M. Teter, A. A. Vikhlinin, R. J. Edgar, M. W. Wise, G. E. Allen, S. N. Virani, J. M. DePasquale, and M. T. Raley, "Flight spectral response of the acis instrument," in *X-Ray and Gamma-Ray Telescopes and Instruments for Astronomy.*, J. Truemper and H. Tananbaum, eds., *Proc. SPIE* **4851**, p. 89, 2003.
13. H. L. Marshall, A. Tennant, C. E. Grant, A. P. Hitchcock, S. L. O'Dell, and P. P. Plucinsky, "Composition of the chandra acis contaminant," in *X-Ray and Gamma-Ray Instrumentation for Astronomy XIII*, K. A. Flanagan and O. H. W. Siegmund, eds., *Proc. SPIE* **5165**, p. 497, 2004.
14. K. Kono, J. G. Sandland, K. Wada, and L. C. Kimerling, "Evaluation of irradiation-induced deep levels in Si," in *Proc. SPIE Vol. 4140, p. 267-273, X-Ray and Gamma-Ray Instrumentation for Astronomy XI, Kathryn A. Flanagan; Oswald H. Siegmund; Eds.*, pp. 267–273, Dec. 2000.